Coupled magneto-mechanical modeling of non-linear ferromagnetic diaphragm systems

V R Jayaneththi*, K C Aw and A J McDaid

Department of Mechanical Engineering, The University of Auckland, Auckland 1010, New Zealand

E-mail*: vjay721@aucklanduni.ac.nz

Abstract

Magnetic polymer composites (MPC) are shape-changing materials capable of wireless actuation. There is growing interest in MPC for biomedical and robotic applications because it removes the need for on-board power systems and electronics. Finite element (FE) methods provide a powerful platform to design and simulate MPC-driven devices. However, the accuracy of previously reported FE MPC models using magnetic body force methods is unknown given the lack of experimental validation.

In this paper, a new finite element model for a soft-magnetic soft diaphragm actuator is proposed and experimentally validated. Here, the geometrical and electrical properties of the electromagnet were explicitly modeled. A comparative study was conducted to validate three well known magneto-mechanical coupling approaches; Maxwell stress tensor and the Kelvin magnetization force, with and without the surface force contribution. In addition, a new method for estimating the nonlinear soft-magnetic properties of MPC was also presented.

Experimental validation revealed the Kelvin magnetization force with surface force contribution resulted in greater simulation accuracy. Using this method, diaphragm deflection was simulated with an RMS error of less than 0.2 mm and a mean absolute error (relative to maximum displacement) well below 10 %, showing good agreement across all recorded trials.

The versatility of the proposed model supports many use cases, ranging from lab-on-a-chip to implantable drug delivery. The generalizable nature of this work also provides the potential for translation to other deformation modes and MPC actuator configurations.

Keywords: magnetic polymer, sensors and actuators, finite elements, elastic material, finite deflections

1. Introduction

Magnetic polymer composites, or MPC, is an emerging class of functional material for biomedical and robotic applications [1]–[3]. MPC, also referred to as magneto-active polymers [4], [5], magpol [1], [6], ferrogel [7], [8] or magnetorheological elastomers [9], [10], undergo shape change in the presence of an external magnetic field. They comprise of a soft polymer matrix with embedded magnetic microparticles. Induced particle interaction forces deform the polymer structure when a magnetic field is applied. Utilizing the wireless capabilities of this flexible transducer may give rise to inherently safer implantable devices and innovative soft robotics that do not require on-board power systems and electronics. Applications of interest include artificial muscle [11], [12], small-scale robotics [3], [13], [14] and drug delivery [15]–[18], to name a few.

MPC modeling is of growing interest due to the challenges posed by the material's nonlinear behavior [19]. As a tool for design and simulation, MPC modeling would enable the rapid development and exploration of novel applications that aim to take advantage of its wireless actuation, fast response and high strain characteristics. Numerous researchers have proposed different methods of modeling MPC, ranging from simple 1-DOF models [20], [21], to continuum-based finite element approaches [22]–[33]. Finite element (FE) modeling is a powerful simulation tool that allows users to model and analyze complex physical systems across multiple physics domains. Recently, a FE framework for modeling hard-magnetic soft materials using magnetic Cauchy stresses was presented [31]. This work, along with similar magnetic Cauchy stress methods [34], have shown promise in this field. Another, more commonly applied, method of modeling magnetically-induced mechanical deformation are magnetic body forces, e.g. the Maxwell stress tensor [35]. Previously reported FE approaches utilizing magnetic body forces have investigated the coupled magneto-mechanical behavior of MPC in, for example, cantilever [22] and peristaltic pump configurations [26], [27], [36]. However, the accuracy of these models remain unknown due to a lack of supporting experimental data. Despite the rising interest in MPC, there is currently no universally accepted FE framework to model deformation. Further experimental analysis is required to shed light on this topic.

MPC actuation performance is partly defined by its magnetic properties. It is common to assume MPC to be a linear magnetic material [37]. Numerous methods in existing literature have detailed how to calculate the relative magnetic permeability of composite materials, either analytically using the Bruggeman or Maxwell-Garnett formula [38], or through coupled finite element approaches [37]. However, the relative permeability of ferromagnetic, or soft-magnetic, materials is not constant and is nonlinearly related to the applied magnetic field. Unlike paramagnetic materials, ferromagnetic materials have microscopic magnetic domains that align, in parallel, to the external magnetic field. This internal magnetization increases magnetic flux density. Magnetic saturation, the field strength at which all domains are aligned, is a property of ferromagnetic (and ferrimagnetic) materials, and its effect cannot be modeled by a single magnetic permeability constant.

Electromagnet design, i.e. geometry and coil properties, also play a vital role in the performance of MPC systems. These two properties greatly affect the strength and shape of the generated magnetic field. With systematic design, an electromagnet can provide the necessary flexibility for an MPC system to adapt to ever changing real world conditions. To date, existing studies rarely account for the electromagnet [27], [28]. The inclusion of this component would allow the overall system to be optimized to specific applications with respect to geometrical and performance constraints, and may be achieved using topology-based optimization techniques or simply, model-guided iterative design.

This paper presents a finite element modeling approach for a soft-magnetic MPC diaphragm actuator. This system is of interest due to its versatility as a decoupled wireless actuator [39]. Potential applications for this soft-magnetic diaphragm actuator include implantable drug delivery pumping, lab-on-chip microfluidic mixing, or as a compliant force transducer for cell manipulation. Diaphragm deformation as a result of the magneto-mechanical interaction between MPC and the inhomogeneous magnetic field generated by an electromagnet is modeled using magnetic body forces. An investigation into the shape deflection of several diaphragm actuators, under different loading conditions, was carried out both experimentally and in simulation to validate the proposed approach. A comparative study of three magneto-mechanical coupling methods (Maxwell stress tensor and Kelvin magnetization force, with and without the surface contribution), was conducted. A coupled FE approach is also presented to determine the nonlinear soft-magnetic properties of MPC.

The main contribution of this work is the proposal and experimental validation of a new FE approach to model soft-magnetic soft diaphragm deformation. The generalizable nature of this work shows potential for translation into alternative deformation modes for soft-magnetic material actuators, and may also provide a general framework for others going forward. In addition, the insights gleaned from this study provide a stepping stone for this work to be extended and applied in the development of novel biomedical and robotic MPC applications.

This paper is structured as follows. In Section 2, an overview of the nonlinear field equations, constitutive equations and magneto-mechanical coupling methods are presented. The implementation of the continuum-based modeling approach is outlined in Section 3. The comparative study of the three coupling methods and overall validation of the FE approach is provided in Section 4. The paper concludes with a discussion of the results in Section 5 and brief remarks in Section 6.

2. Theory

2.1. Electromagnetic constitutive laws and field theory

The kinematics of deformable continua and the basic principles of continuum mechanics are already well established in literature and will be not be covered here [35], [40]. A brief overview of the constitutive laws and equations relating to electromagnetism are provided for context.

In the presence of an external magnetic field, a ferromagnetic material will become magnetized. The following constitutive relationship describes this induced magnetic flux density, $\boldsymbol{B}$, for ferromagnetic materials,

$$\boldsymbol{B} = \mu_0(\boldsymbol{H} + \boldsymbol{M}) \tag{1}$$

This behavior is generally characterized by a magnetization curve measured using vibrating sample magnetometry. This process measures the magnetization, $\boldsymbol{M}$, of a material when exposed to an external magnetic field, $\boldsymbol{H}$. For ferromagnetic materials, this curve can be approximated by a sigmoid function [41]. Note, hysteretic effects in MPC are considered negligible due to the low mass fraction of magnetic particles [42]. The magnetization (MH) curve for MPC can be expressed as follows,

$$M = M_\infty tanh(kH) \tag{2}$$

Where, M_∞ is the saturation magnetization (A/m) and k is the rate of magnetization.

A magnetic field can be described classically using Maxwell's equations. Assuming the electric field is negligible and the system is quasi-static (i.e. change in electric flux density over time is zero), the magnetic field and its interactions can be defined by the following two expressions,

$$\nabla \times \boldsymbol{H} = \boldsymbol{J_e} \tag{3}$$
$$\nabla \cdot \boldsymbol{B} = 0 \tag{4}$$

Where Eq. (3) is Ampere's Law, where $\boldsymbol{J_e}$ is the external current density generated by the electromagnet, and Eq. (4) is Gauss' Law for Magnetism.

When energized, the electromagnet applies an external current density in the direction of the coil windings. This current density can be approximated using the following expression,

$$\boldsymbol{J_e} = \frac{NI_{coil}}{A} \tag{5}$$

Where N is the number of coil turns, I_{coil} is the coil current, and A is the cross sectional area of the coil.

2.2. Finite hyperelasticity theory

Strain energy density functions are often employed to describe the stress response of non-linear elastic materials e.g. rubber, biological tissue. Here, the Ogden model is used to model the macroscopic mechanical behavior of MPC [43]. The postulated strain energy function, derived by Ogden, is a

function of the principal stretches,λ_{1-3}, and is expressed below. Similar to other rubber-like materials, MPC is assumed to be 3rd order, isotropic and incompressible i.e. $\lambda_1\lambda_2\lambda_3 = 1$ [40]. Note, μ_p are the shear moduli and α_p are dimensionless constants.

$$\psi = \psi(\lambda_1, \lambda_2, \lambda_3) = \sum_{p=1}^{N} \frac{\mu_p}{\alpha_p} (\lambda_1^{\alpha_p} + \lambda_2^{\alpha_p} + \lambda_3^{\alpha_p} - 3) \quad (6)$$

Where,

$$N = 3, and\ p = 1, \dots, N$$

2.3. Magneto-mechanical coupling

In literature, the two most common magnetic body force, or magneto-mechanical coupling methods are the Maxwell stress tensor and Kelvin magnetization force. The latter is more commonly used for ferrohydrodynamics [44], [45]. In this paper, both are implemented to validate each approach as it is not known which will perform better.

2.3.1. Maxwell Stress Tensor

The Maxwell stress tensor is given by the following expression [46], where B is the flux density, μ_0 is the magnetic permeability of free space and δ_{ij} is the kronecker delta. The indices i and j refer to the coordinate directions.

$$\boldsymbol{T}_{Maxwell} = \mu_0^{-1}(B_i B_j - \frac{1}{2} B^2 \delta_{ij}) \quad (7)$$

The resultant force on a body is found by integrating the Maxwell stress tensor over its surface, S, and is given by the following expression,

$$F_{Maxwell} = \oint_S \boldsymbol{T}_{Maxwell}\, dA \quad (8)$$

2.3.2. Kelvin Magnetization Force

The magnetizable filler material in MPC can be thought of as microscopic dipoles that experience an electromagnetic force when an external magnetic field gradient is applied. This force can be calculated using the Kelvin formulation [47]. The total force acting on a magnetizable material can be described by the summation of the body and surface contributions,

$$F_{Kelvin} = F_{Kelvin,volume} + F_{Kelvin,surface} \quad (9)$$

Where,

$$F_{Kelvin,volume} = \int_V \mu_0 (\boldsymbol{M}.\nabla)\boldsymbol{H} dV \tag{10}$$

$$F_{Kelvin,surface} = \oint_S \frac{\mu_0}{2} (\boldsymbol{M_{norm}})^2 dA \tag{11}$$

Where, $\boldsymbol{M}$ is the magnetization of the body, $\boldsymbol{M_{norm}}$ is the magnetization normal to the surface, and $\boldsymbol{H}$ is the external magnetic field. Note, previous MPC literature have ignored the surface contribution. The influence of this term will be explored in this paper.

Expanding the convective operator, the volumetric component of the Kelvin force (or body force density), with respect to a cylindrical coordinate frame, can be expressed as follows; assuming the azimuthal force in the diaphragm actuator can be ignored (due to axial symmetry),

$$\begin{bmatrix} f_{Kelvin,r} \\ f_{Kelvin,z} \end{bmatrix} = \begin{bmatrix} \mu_0 (M_r \frac{\partial H_r}{\partial r} + M_z \frac{\partial H_r}{\partial z}) \\ \mu_0 (M_r \frac{\partial H_z}{\partial r} + M_z \frac{\partial H_z}{\partial z}) \end{bmatrix} \tag{12}$$

Herein, the Kelvin magnetization force without surface contribution, with surface contribution, and Maxwell stress tensor will be referred to as K1, K2 and K3, respectively.

3. Finite element implementation

The configuration of the soft-magnetic soft diaphragm actuator was proposed in previous work [21]. This decoupled system consists of a clamped, pre-tensioned magnetic diaphragm that is wirelessly actuated by an electromagnet. When the electromagnet is energized, the magneto-mechanical interaction between the inhomogeneous magnetic field and magnetic microparticles cause the diaphragm to deflect. The diaphragm is pre-tensioned to provide an elastic restoring force when the field is removed. Nonlinearities arise because the resultant magnetic forces are a function of not only field gradient, but also diaphragm deformation [21]. In this study, diaphragm deformation was assumed to be symmetrical about the z axis (azimuthal symmetry), thus a 2D axisymmetric approximation was considered sufficient to simulate the system. An overview of the actuator and 2D axisymmetric representation of the system is illustrated in Figure 1. The finite element model was implemented in COMSOL Multiphysics 5.3 (COMSOL Inc., Sweden).

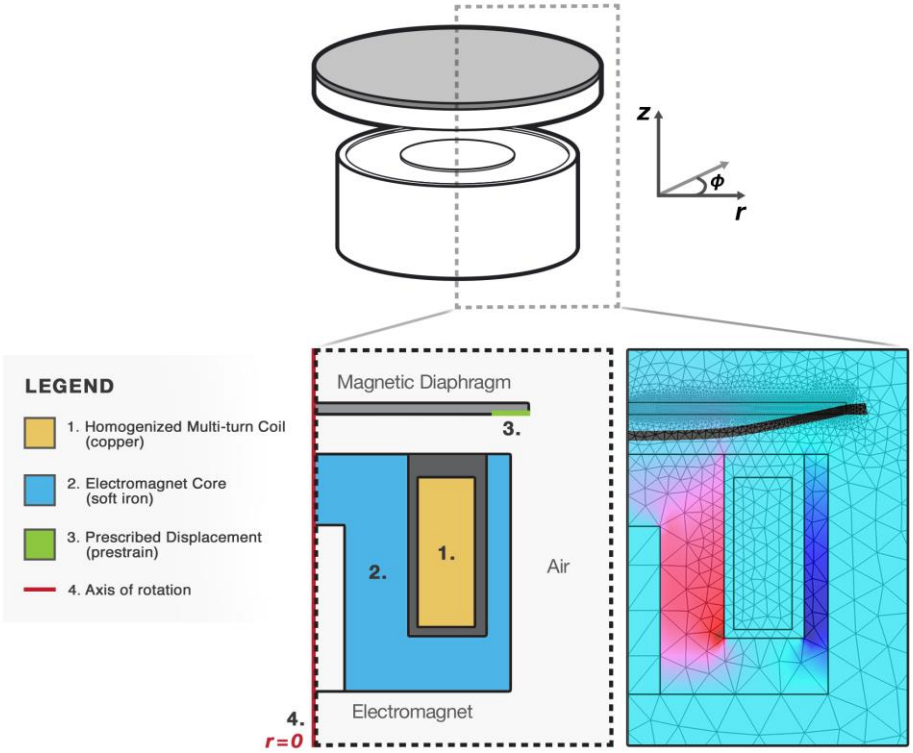

Figure 1: The proposed actuator configuration; the electromagnet is located below the magnetic diaphragm. When the electromagnet is energized, the diaphragm deflects downwards. It is assumed deformation is axisymmetric. The geometry of the 2D axisymmetric model for the system is also illustrated. The electromagnet is modeled as a homogenized multi-turn coil and the diaphragm as a hyperelastic material. A prescribed displacement (highlighted in green) applies a pre-strain to the diaphragm. A snapshot of the deformed geometry is also illustrated for reference.

The MPC diaphragm was modeled as a hyperelastic material (3rd order Ogden material model). The ferromagnetic properties of the diaphragm (and electromagnet core) were defined by the following constitutive relationship, characterized by the material's HB curve, which is derived from the magnetization curve,

$$|\boldsymbol{H}| = f(|\boldsymbol{B}|) \tag{13}$$

The Kelvin magnetization force and resultant force due to the Maxwell stress tensor were applied as magnetic body loads on the diaphragm. The surface contribution of the Kelvin force was applied as a boundary load. Gravitational forces were also accounted for. The diaphragm was pre-tensioned by applying a prescribed displacement at the outer edge. Here, Green-Lagrange strain was used to model geometric nonlinearities due to hyperelastic material deformation.

An unstructured mesh grid with triangular 3-node elements allowed for a finer resolution at the boundaries of the diaphragm whilst minimizing computation time. An infinite element domain was applied to the outer air domain boundary to account for the far magnetic field region. To prevent mesh distortion and improve accuracy, a moving mesh was also applied to the geometry surrounding the

TABLE I
ELECTROMAGNET MODELS

Electromagnet	Model	Outer Diameter (mm)	Core Diameter (mm)
EM1	GMHX30	30	14
EM2	GMHX40	40	19
EM3	GMHX50	50	24

diaphragm using the arbitrary Lagrangian-Eulerian method. Winslow mesh smoothing was applied to these elements undergoing free deformation [48]. Lastly, a mesh refinement study was conducted to ensure the solutions reached convergence. The resulting maximum element size for the diaphragm and neighboring air domain elements was set to 0.3 mm.

In total, six actuator configurations were modeled; two diaphragms (45 and 60 mm diameter) with three electromagnets (Magnet Schultz Ltd, UK) of increasing size, summarized in Table 1. The mean (SD) number of domain and boundary elements for the 45 and 60 mm diaphragm configurations were 3362 (38) and 319 (3), and 4182 (54) and 365 (2), respectively. The damped Newton method was utilized to solve this time-varying, nonlinear multiphysics problem [49].

4. Model Validation

4.1. Electromagnet characterization

Firstly, to validate the FE electromagnet models, the flux density along the top surface of each electromagnet was measured. The coil current was fixed at 0.40 A, 0.80 A and 0.85 A for EM1, EM2 and EM3, respectively. A gauss meter (Model GM2, AlphaLab Inc., USA) was used to measure the flux density, B_z, along a single axis, at 4 mm intervals and once at the center. The internal geometry and coil properties were determined by taking the cross section of each device.

The simulated flux density along the top surface of EM3 is provided in Figure 2 as a representative example. The simulated flux closely emulates the experimental measurements for each electromagnet. The root mean square error (RMSE) for EM1, EM2 and EM3 was 0.0034, 0.0062 and 0.0072 T, respectively.

4.2. Material fabrication

MPC is composed of a polymer matrix and magnetic filler. In this study, the two constituents were silicone rubber (Ecoflex 00-30, Smooth-On, USA) and a soft-magnetic filler (Synthetic Fe_3O_4, Inoxia Ltd, UK). The following fabrication process was adapted from previous work [21]. Here, the mass fraction of magnetic filler was 20 wt%. To begin, the uncured silicone and powdered magnetic filler were thoroughly mixed using a planetary mixer (Mazerustar KK-50S, Kurabo, Japan). The composite

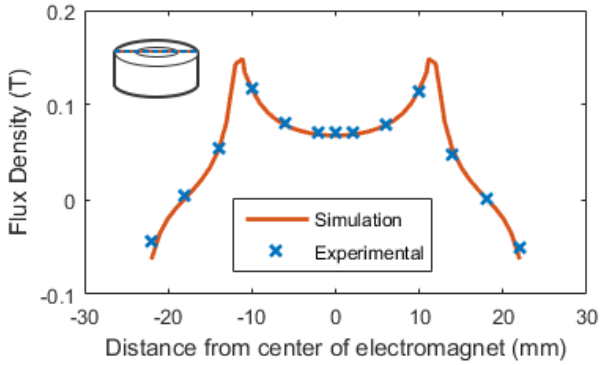

Figure 2: Representative example of the simulated vs measured flux density, B_z, along the top surface for EM3

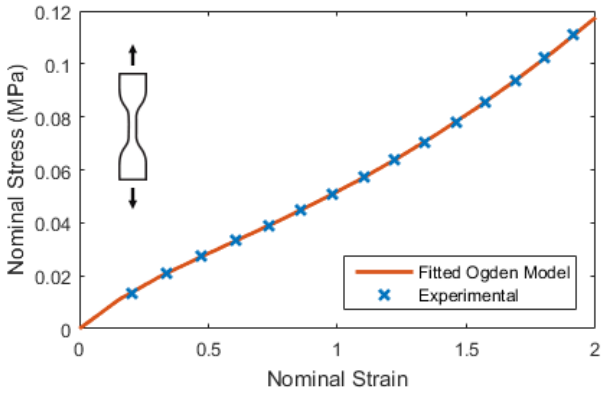

Figure 3: Hyperelastic curve fitting, Ogden model vs experimental stress-strain data for the 20 wt% MPC material

TABLE 2
FITTED HYPERELASTIC (OGDEN) MODEL PARAMETERS

Constant	Value (MPa)	Constant	Value
μ_1	-0.194	α_1	2.19
μ_2	0.180	α_2	2.44
μ_3	4.23 x 10^{-2}	α_3	0.207

was cast into a mold and degassed in a vacuum chamber for 10 minutes to remove trapped air. The samples were left to cure in an oven, at 80°C, for one hour. The thickness of each sample was 1.5 mm. Once cured, the samples were pre-strained to 10%. In this study, two MPC diaphragm diameters of interest were tested to investigate the effect of changing sample geometry on model accuracy. The diameter of each diaphragm, once pre-tensioned, was 45 and 60 mm.

4.3 Material characterization

The mechanical and nonlinear magnetic properties of the MPC material were identified using a combined modeling approach (experiments and simulation).

4.3.1. Mechanical properties

To determine the stress-strain relationship of MPC, uniaxial tensile testing was carried out in accordance with ASTM-D412 [50]. The material was tested using an Instron 5567 (Illinois Tool Works Inc., MA, USA). The 'Test Method A: Dumbbell Straight Section Specimens' protocol was followed with an applied strain rate of 500 mm/min. Test samples were fabricated using Die C, with a material thickness of 3 mm. A nonlinear least squares solver was used to fit the hyperelastic parameters to the recorded test data (Abaqus curve fitting tool, Dassault Systèmes, France).

The stress-strain relationship and fitted hyperelastic model for the MPC material is presented in Figure 3. It is evident the gradient of the stress-strain relationship is not constant (as with linear-elastic materials) and thus supports the assumption that the MPC material is hyperelastic. The fitted material constants for the 3rd order Ogden model are provided in Table 2.

4.3.2. Magnetic properties

Existing methods to estimate the magnetic properties, namely relative permeability, include, the Maxwell-Garnett mixing rule or induction measurements with a combined finite element approach. Here, an alternative FE modeling approach to characterize the magnetic properties of MPC is presented. The following parameter identification process utilizes displacement data and FE analysis.

The magnetic properties, M_∞ and k, for the 45 and 60 mm samples were optimized by minimizing the sum of squares between simulated and measured maximum diaphragm displacement. For this, time-varying ramp data was used; the experimental protocol is outlined in Section 4.4. Ideally, the magnetic properties for the 45 and 60 mm samples should be identical because the mass fraction of magnetic filler is kept constant. To evaluate if model overfitting was also present, data from only one electromagnet configuration, i.e. EM2, was used for optimization. If overfitting is present, there will be greater relative error between the experimental and simulated results for both EM1 and EM3.

The MH curve parameters were optimized using each coupling method (K1, K2, K3), for each diaphragm diameter (45 and 60 mm). The effect of assuming linear versus nonlinear magnetic properties was also investigated. A representative example of the optimized displacement plots is provided in Figure 4. The simulations are in good agreement with the measured displacement, for all coupling methods, when nonlinear magnetic properties are assumed. The RMS errors are summarized in Table 3. In all cases, the RMS error was approximately three times greater when linear magnetic properties were assumed. These results support the notion that MPC should be modeled as a nonlinear magnetic material.

The optimized magnetic parameters are presented in Figure 5. M_∞ and k, are similar for both the 45 and 60 mm samples when using the Kelvin magnetization force, with (K1) and without (K2) the surface contribution. The optimized magnetic permeability (μ_r) was also similar for both samples when using

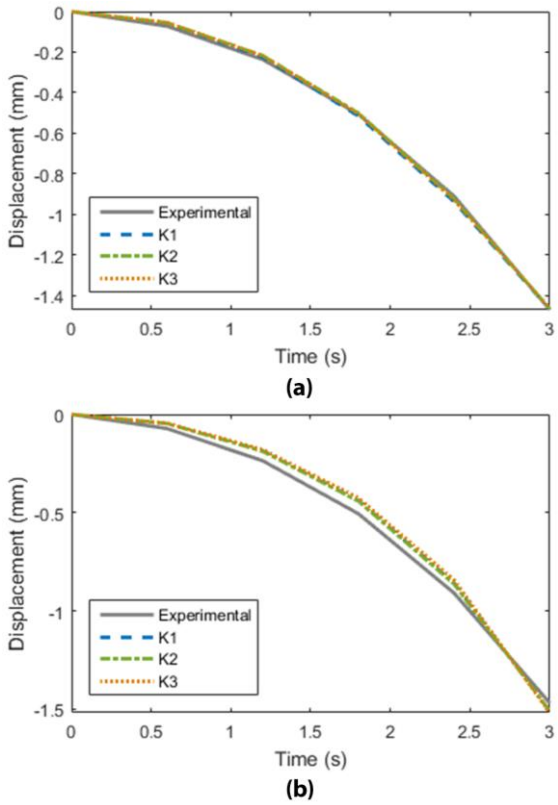

Figure 4: Representative example of diaphragm displacement at P1 for the 60 mm diameter, EM2 configuration, following optimization of a) nonlinear (MH) and b) linear (constant relative permeability) magnetic properties. Note, K1, K2 and K3 are the Kelvin magnetization force (without surface contribution), with surface contribution, and Maxwell stress tensor methods, respectively.

TABLE 3
SUMMARY OF ERROR FOR OPTIMIZED TRIALS

Method	Diaphragm (mm)	RMSE (mm)	
		Nonlinear	Linear
$K1$	45	0.0059	0.0162
	60	0.0141	0.0446
$K2$	45	0.0054	0.0161
	60	0.0122	0.0424
$K3$	45	0.0054	0.0161
	60	0.0134	0.0537

K1 and K2. For M_∞ and k, the magnitude of the estimated parameters for the 60 mm sample were noticeably greater when using K3.

4.4. Surface deflection analysis

To validate the proposed FE modeling approach, the surface deflection of each diaphragm actuator was measured. A single surface measurement (i.e. center displacement) is not sufficient to evaluate the model's performance, especially when shape is of interest. Here, multiple measurements were taken to

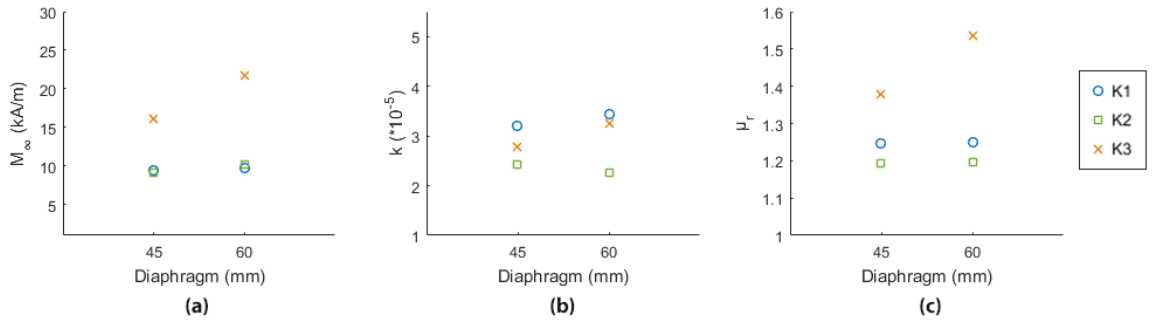

Figure 5: The optimized magnetic properties for the 20 wt% MPC material; a) Magnetic saturation, M_{∞}, and b) rate of magnetization, k, are nonlinear magnetic properties. For completeness, the optimized relative magnetic permeability (which assumes linear behavior) is also presented in c). Note, the upper and lower bounds for optimization are represented by the vertical axes.

understand how electromagnet (and diaphragm) geometry affects diaphragm deformation. The system is also subjected to varying magnetic fields (spatial, magnitude) to assess model generalizability.

In this study, three electromagnets of varying size were used to validate the FE modeling approach (EM1, EM2, and EM3). The voltage applied across each electromagnet was limited to 20, 20 and 25 V, respectively. The resulting maximum flux density, B_z, was 0.12, 0.15 and 0.21 T, respectively. Diaphragm surface deflection was measured at six discrete points using a scanning laser Doppler vibrometer (PSV-500, Polytec GmbH, Walbronn, Germany). The displacement at each point was sampled at 1 kHz. Due to azimuthal symmetry, diaphragm deflection could be reconstructed from these six points, aptly named P1 – P6. An overview of the experimental setup is illustrated in Figure 6. When energized, the diaphragm deflects down, towards the electromagnet. The gap distance i.e. distance between the bottom surface of the diaphragm and top surface of the electromagnet, was set to 5 mm. This distance, determined by referring to previously published work [21], allowed for relatively large diaphragm deflection without impacting the electromagnet.

Three trials were conducted on each diaphragm-electromagnet configuration. For each trial, the electromagnet was energized with a different input signal; ramp, 1 Hz sinusoid and 2 Hz sinusoid. The duration of the trials were 3, 5 and 5 seconds, respectively.

This study also investigated the accuracy of the three magneto-mechanical coupling methods (K1, K2, K3). Each trial was simulated using the respective nonlinear magnetic and mechanical material properties derived in Section 4.3. A representative example of the simulation vs experimental results is illustrated in Figure 7. The experimental and simulated maximum displacement for each configuration, recorded during the ramp trials, is summarized in Table 4. The RMS error and mean absolute error (MAE) was calculated for individual measurement points (P1 – P6), for each trial. These results are collated and presented in Figure 8. In general, maximum displacement occurred at P1 (the center of each diaphragm). Displacement increased with increasing field strength, regardless of diaphragm diameter. Model accuracy also appears to be independent of diaphragm diameter, highlighted by similar

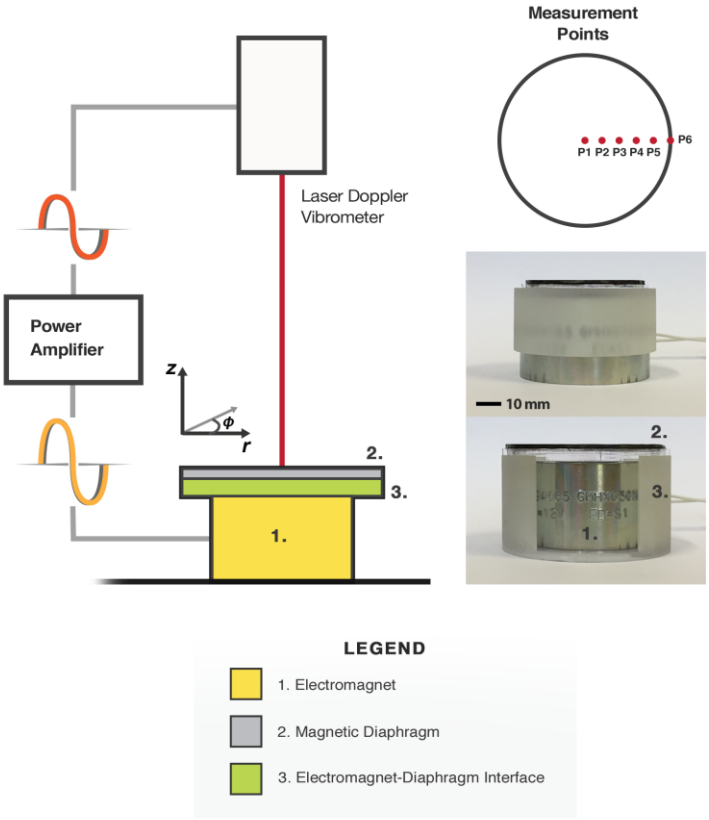

Figure 6: A laser Doppler vibrometer (LDV) measured the surface deflection of each magnetic diaphragm at six discrete points. Three trials were carried out for each diaphragm-electromagnet configuration. The electromagnet was energized with a different input waveform (ramp, 1 Hz sinusoid, 2 Hz sinusoid) for each trial. Waveforms generated by the LDV were amplified by an external power amplifier. In total, six actuator permutations were tested (two diaphragms and three electromagnets). The gap distance, i.e. distance between the top surface of the electromagnet and bottom surface of the diaphragm, was fixed at 5 mm. The EM3 configuration for the 45 mm (top) and 60 mm (bottom) diaphragms are pictured to the right.

relative differences in Table 4, suggesting experimental-simulation discrepancies were mostly influenced by the applied coupling method.

In summary, K2 had the lowest mean RMS error across all six points, across all trials. The RMS error, for all points, was below 0.2 mm for both K1 and K2. MAE, relative to maximum measured displacement, was less than 10% for both K1 and K2. As expected, all three coupling methods are capable of simulating the system response with low error following optimization (i.e. EM2 configuration), evident in Figure 7 and Table 4. However, it can be observed that K3 has poorer shape deflection accuracy closer to the clamped edge of the diaphragm, clearly illustrated in Figure 7b.

A true measure of model performance can be determined by cross validating against datasets not optimized for i.e. EM1 and EM3 configurations. At weaker magnetic field strengths (EM1), K1 tended to overestimate surface deflection. At greater magnetic field strengths (EM3), K1 underestimated surface deflection. The opposite was true for K3 in both cases. K2 was consistent across all datasets and, overall, was the best modeling approach. The low error across all trials for K2 also suggests the

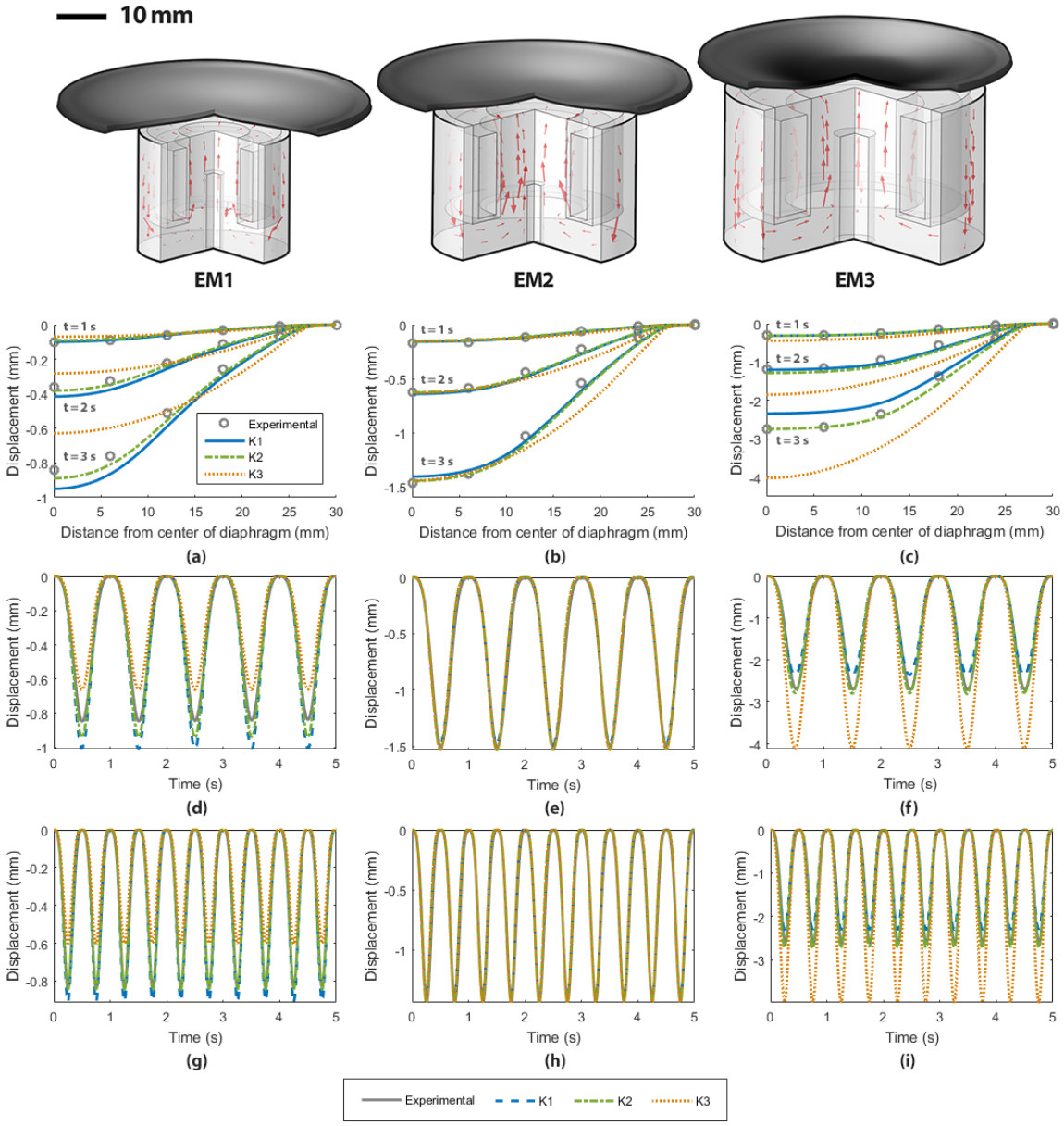

Figure 7: Representative example of the shape deflection plots (simulated vs experimental) for the 60 mm diaphragm. Surface deflection during the ramp trial, at different time steps, for the a) EM1, b) EM2 and c) EM3 configurations. The displacement of P1 (diaphragm center) during the 1 Hz sinusoidal trial for d) EM1, e) EM2, f) EM3, and 2 Hz sinusoidal trial for g) EM1, h) EM2 and i) EM3. Note, the magnetic properties were optimized using ramp trial data from a single point (P1), from the EM2 configuration. The maximum simulated displacement for the 60 mm diaphragm during each ramp trial is illustrated (top) for comparison.

proposed model is not overfit and corroborates the use of nonlinear magnetic properties for modeling MPC.

5. Discussion

In this paper, we have presented a finite element approach for modeling magnetic diaphragm deformation. Here, the physical geometry and coil properties of the electromagnet were modeled in conjunction with the mechanical and magnetic properties of the diaphragm. Three methods of coupling

TABLE 4
MAXIMUM DIAPHRAGM DISPLACEMENT FOR EACH CONFIGURATION

Electromagnet	Diaphragm (mm)	Maximum Displacement – Relative Difference (%)			
		Experimental (mm)	K1	K2	K3
EM1	45	0.476	+21.43	+17.23	-24.58
	60	0.840	+22.02	+14.52	-19.52
EM2*	45	0.725	+3.31	+4.00	+4.18
	60	1.471	+1.70	+5.17	+4.89
EM3	45	1.094	-6.95	+1.01	+60.24
	60	2.756	-12.7	+2.36	+50.4

*Optimized dataset

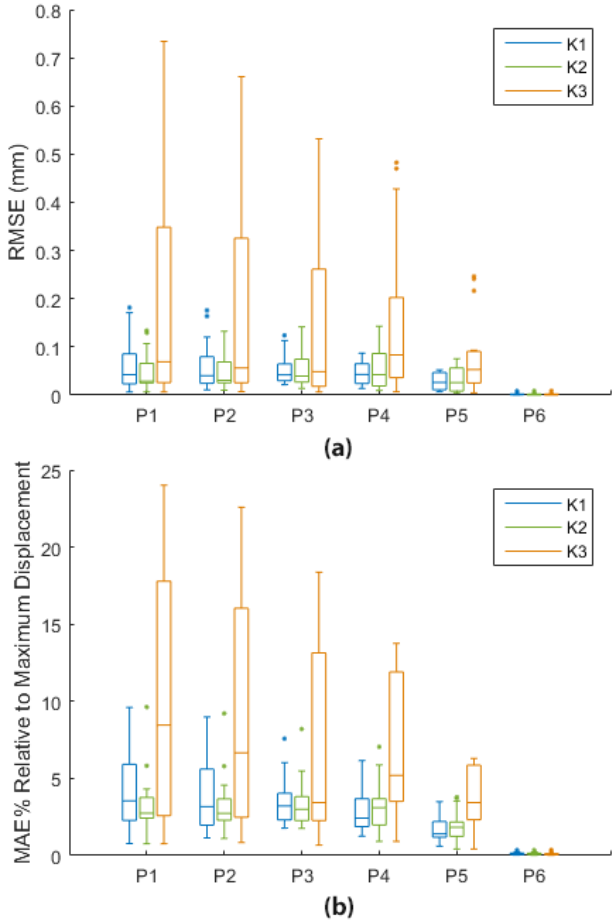

Figure 8: A comparison of the a) RMS error and b) mean absolute error (% relative to measured maximum diaphragm displacement for each configuration) for each point across all trials (18 in total).

the magnetics and structural mechanics domains were investigated. While both Kelvin magnetization force methods adhered closely to experimental data, accounting for the surface contribution (K2) resulted in the lowest error, overall. The proposed approach offers a generalizable tool for accurate shape deformation modeling of soft-magnetic diaphragm materials. The insights gleaned regarding

magneto-mechanical coupling methods will be of interest to those simulating deformation of magnetic particle-loaded elastomers.

Clamped MPC diaphragm deformation was the focus of this study. The lack of prior experimental validation of existing multiphysics approaches justify the analysis of this relatively simple configuration. Here, simulated shape deformation was validated using a comprehensive set of experimental data. In addition, the versatility of the presented diaphragm configuration also supports many use cases, ranging from, for example, lab-on-a-chip applications to implantable drug delivery. Because both MPC and electromagnet behavior was simulated, an interesting use for this model would be topology-based optimization, where geometrical (and/or power) constraints are imposed on the system design. When spatial constraints are present, the interaction between the electromagnet and soft-magnetic material is especially important because dipole magnetic fields obey the inverse cube law at large distances.

It is common, in existing literature, to assume linear magnetic properties for MPC materials. In this paper, a universal approach to estimate the nonlinear magnetic properties of MPC was proposed. An isotropic soft-magnetic material was characterized using measured displacement data and finite element simulations. It was shown the constant relative permeability assumption led to increased error when simulating MPC deformation. Accounting for magnetization effects, such as magnetic saturation, resulted in improved model accuracy.

Consistent magnetic parameters were estimated and low simulation errors were achieved when using the Kelvin magnetization force (with or without the surface force contribution). The same could not be said regarding the Maxwell stress tensor. There are numerous studies that have compared the Kelvin formula and Maxwell stress tensor [44], [51]–[53]. In general, each method predicts similar forces. The difference lies in how each force is calculated. The Maxwell method calculates the global force whereas the Kelvin formulation provides local body forces [47], [54]. In this study, the effects of this difference appear to become more pronounced at larger diaphragm deformations, and may explain why the error is greater when using the Maxwell stress tensor method. In addition, including the surface contribution for the Kelvin formula resulted in improved model accuracy. It is often assumed that surface forces are negligible and can be ignored, however, the reported findings indicate surface forces should be considered when modeling soft-magnetic soft material deformation.

K2 was established as the best magneto-mechanical coupling method. Knowing this, it was observed that relative model accuracy improved when modeling larger electromagnets, highlighted in Table 4. Simulating geometrically larger coils led to lower relative differences, regardless of displacement. This observation may be explained by resistive heating. When energized for extended periods of time, electromagnet temperature and coil resistance increases. This ultimately leads to a degraded magnetic field. Smaller electromagnets may be more susceptible to thermal effects because there is less surface

area to dissipate heat. Although efforts were taken to reduce resistive heating, by limiting trial length and implementing cool down periods, thermal effects were not accounted for in the proposed model.

The accuracy of the hyperelastic material model can be further improved by using additional experimental data. For this study, only uniaxial tensile test data was utilized. It is suggested that biaxial and planar experimental data also be included to better capture the range of deformation modes experienced by the diaphragm. In addition, the strain rate applied during uniaxial testing, in accordance with ASTM-D412, may not reflect the strain rate experienced by the diaphragm during use. Due to viscoelasticity, the material's stress-strain performance is also affected by strain rate. A more appropriate rate should be considered for future experiments.

The effects of disturbances and non-magnetic loading conditions on actuator response and model accuracy were not investigated. This paper focused on diaphragm deformation as a result of magneto-mechanical interaction. To better understand the force transduction capabilities of the soft-magnetic soft diaphragm actuator, future work should couple the proposed approach with, for example, computational fluid dynamics, to model realistic use cases, such as, diaphragm pumping. This work has also revealed that the Kelvin magnetization force (with surface force contribution) results in the greatest model accuracy. It is suggested that alternative deformation modes e.g. cantilever bending, also be investigated using this newly obtained insight into MPC modeling.

6. Conclusions

This paper presents a finite element approach for modeling soft deformation in ferromagnetic diaphragm systems. Surface deflection analysis was carried out to experimentally validate the model. An investigation into different magneto-mechanical coupling methods revealed the Kelvin magnetization force (with surface force contribution) provided the highest model accuracy. A new method for characterizing nonlinear magnetic properties of MPC was also proposed.

The proposed finite element approach takes into account both the diaphragm and electromagnet. This presents a powerful simulation tool for MPC applications where strict geometrical and power constraints must be adhered to. In addition, this modeling approach opens up the opportunity for topological optimization of MPC-based systems. The proposed model can be expanded and coupled with, for example, computational fluid dynamics, to explore potential wireless force transduction applications. Future work should also explore alternative deformation modes e.g. cantilever bending, given the new insights on magneto-mechanical coupling methods.

Acknowledgements

This research was supported in part by the Engineers in Clinical Residence Programme administered by the "Technologies for Health" Theme from The University of Auckland. In addition, the authors would like to thank Marshall Lim, Logan Stuart, and Sarath Pathirana for their technical expertise and assistance with the experimental protocols.

References

[1] V. Q. Nguyen, A. S. Ahmed, and R. V. Ramanujan, "Morphing soft magnetic composites," *Adv. Mater.*, vol. 24, no. 30, pp. 4041–4054, 2012.

[2] J. Thévenot, H. Oliveira, O. Sandre, and S. Lecommandoux, "Magnetic responsive polymer composite materials.," *Chem. Soc. Rev.*, vol. 42, no. 17, pp. 7099–116, 2013.

[3] Y. Kim, H. Yuk, R. Zhao, S. A. Chester, and X. Zhao, "Printing ferromagnetic domains for untethered fast-transforming soft materials," *Nature*, vol. 558, no. 7709, pp. 274–279, Jun. 2018.

[4] L. A. Makarova *et al.*, "Magnetoactive elastomer as an element of a magnetic retina fixator," *Smart Mater. Struct.*, vol. 26, no. 9, p. 95054, Sep. 2017.

[5] P. von Lockette, "Fabrication and Performance of Magneto-Active Elastomer Composite Structures," in *Volume 1: Development and Characterization of Multifunctional Materials; Modeling, Simulation and Control of Adaptive Systems; Structural Health Monitoring; Keynote Presentation*, 2014, p. V001T01A019.

[6] A. S. Ahmed and R. V. Ramanujan, "Bio inspired Magnet-polymer (Magpol) actuators," in *Proceedings of SPIE - The International Society for Optical Engineering*, 2014, vol. 9055, p. 90550O.

[7] M. Zrínyi, L. Barsi, and A. Büki, "Ferrogel: a new magneto-controlled elastic medium," *Polym. Gels Networks*, vol. 5, no. 5, pp. 415–427, 1997.

[8] R. V Ramanujan and L. L. Lao, "The mechanical behavior of smart magnet–hydrogel composites," *Smart Mater. Struct.*, vol. 15, no. 4, p. 952, 2006.

[9] S. Kashima, F. Miyasaka, and K. Hirata, "Novel soft actuator using magnetorheological elastomer," in *IEEE Transactions on Magnetics*, 2012, vol. 48, no. 4, pp. 1649–1652.

[10] T. Yildirim, M. H. Ghayesh, W. Li, and G. Alici, "Nonlinear dynamics of a parametrically excited beam with a central magneto-rheological elastomer patch: An experimental investigation," *Int. J. Mech. Sci.*, vol. 106, pp. 157–167, Feb. 2016.

[11] A. S. Ahmed and R. V. Ramanujan, “Hysteretic Buckling for Actuation of Magnet-Polymer Composites,” *Macromol. Chem. Phys.*, vol. 216, no. 15, pp. 1594–1602, Aug. 2015.

[12] F. Fries, S. Miyashita, D. Rus, R. Pfeifer, and D. D. Damian, “Electromagnetically driven elastic actuator,” in *2014 IEEE International Conference on Robotics and Biomimetics, IEEE ROBIO 2014*, 2014, pp. 309–314.

[13] W. Hu, G. Z. Lum, M. Mastrangeli, and M. Sitti, “Small-scale soft-bodied robot with multimodal locomotion,” *Nature*, vol. 554, no. 7690, pp. 81–85, Jan. 2018.

[14] S. de Pedro *et al.*, “PDMS-based, magnetically actuated variable optical attenuators obtained by soft lithography and inkjet printing technologies,” *Sensors Actuators A Phys.*, vol. 215, pp. 30–35, Aug. 2014.

[15] F. Munoz, G. Alici, H. Zhou, W. Li, and M. Sitti, “Analysis of Magnetic Interaction in Remotely Controlled Magnetic Devices and Its Application to a Capsule Robot for Drug Delivery,” *IEEE/ASME Transactions on Mechatronics*, pp. 1–1, 2017.

[16] F. N. Pirmoradi, J. K. Jackson, H. M. Burt, and M. Chiao, “A magnetically controlled MEMS device for drug delivery: design, fabrication, and testing,” *Lab Chip*, vol. 11, no. 18, p. 3072, Sep. 2011.

[17] F. N. Pirmoradi, J. K. Jackson, H. M. Burt, and M. Chiao, “On-demand controlled release of docetaxel from a battery-less MEMS drug delivery device,” *Lab Chip*, vol. 11, no. 16, p. 2744, Aug. 2011.

[18] M. M. Said, J. Yunas, R. E. Pawinanto, B. Y. Majlis, and B. Bais, “PDMS based electromagnetic actuator membrane with embedded magnetic particles in polymer composite,” *Sensors Actuators A Phys.*, vol. 245, pp. 85–96, 2016.

[19] M. A. Cantera, M. Behrooz, R. F. Gibson, and F. Gordaninejad, “Modeling of magneto-mechanical response of magnetorheological elastomers (MRE) and MRE-based systems: a review,” *Smart Mater. Struct.*, vol. 26, no. 2, p. 23001, Feb. 2017.

[20] Y. Yu, Y. Li, and J. Li, “Parameter identification and sensitivity analysis of an improved LuGre friction model for magnetorheological elastomer base isolator,” *Meccanica*, vol. 50, no. 11, pp. 2691–2707, Nov. 2015.

[21] V. Jayaneththi, K. C. Aw, and A. J. McDaid, “Design-based modeling of magnetically actuated soft diaphragm materials,” *Smart Mater. Struct.*, Feb. 2018.

[22] R. Sheridan, J. Roche, S. E. Lofland, and P. R. vonLockette, “Numerical simulation and experimental validation of the large deformation bending and folding behavior of magneto-

active elastomer composites," *Smart Mater. Struct.*, vol. 23, no. 9, p. 94004, Sep. 2014.

[23] A. Attaran, J. Brummund, and T. Wallmersperger, "Modeling and finite element simulation of the magneto-mechanical behavior of ferrogels," *J. Magn. Magn. Mater.*, vol. 431, pp. 188–191, Jun. 2017.

[24] Y. L. Raikher, O. V Stolbov, and G. V Stepanov, "Shape instability of a magnetic elastomer membrane," *J. Phys. D. Appl. Phys.*, vol. 41, no. 15, p. 152002, 2008.

[25] P. von Lockette, S. E. Lofland, J. Biggs, J. Roche, J. Mineroff, and M. Babcock, "Investigating new symmetry classes in magnetorheological elastomers: cantilever bending behavior," *Smart Mater. Struct.*, vol. 20, no. 10, p. 105022, Oct. 2011.

[26] M. Behrooz and F. Gordaninejad, "A flexible micro fluid transport system featuring magnetorheological elastomer," *Smart Mater. Struct.*, vol. 25, no. 2, p. 25011, Feb. 2016.

[27] A. Ehsani and A. Nejat, "Conceptual design and performance analysis of a novel flexible-valve micropump using magneto-fluid-solid interaction," *Smart Mater. Struct.*, vol. 26, no. 5, p. 55036, May 2017.

[28] S. Murao, K. Mitsufuji, K. Hirata, and F. Miyasaka, "Coupled Analysis by Viscoelastic Body with Rigid Body for Design of MRE Soft Actuator," *Electr. Eng. Japan*, vol. 203, no. 3, pp. 30–38, May 2018.

[29] M.-A. Keip and M. Rambausek, "Computational and analytical investigations of shape effects in the experimental characterization of magnetorheological elastomers," *Int. J. Solids Struct.*, vol. 121, pp. 1–20, Aug. 2017.

[30] J. Maas and D. Uhlenbusch, "Experimental and theoretical analysis of the actuation behavior of magnetoactive elastomers," *Smart Mater. Struct.*, vol. 25, no. 10, p. 104002, Oct. 2016.

[31] R. Zhao, Y. Kim, S. A. Chester, P. Sharma, and X. Zhao, "Mechanics of Hard-Magnetic Soft Materials," *J. Mech. Phys. Solids*, Oct. 2018.

[32] P. Gebhart and T. Wallmersperger, "A general framework for the modeling of porous ferrogels at finite strains," *J. Mech. Phys. Solids*, vol. 122, pp. 69–83, Jan. 2019.

[33] S. V. Kankanala and N. Triantafyllidis, "On finitely strained magnetorheological elastomers," *J. Mech. Phys. Solids*, vol. 52, no. 12, pp. 2869–2908, Dec. 2004.

[34] K. Danas, S. V. Kankanala, and N. Triantafyllidis, "Experiments and modeling of iron-particle-filled magnetorheological elastomers," *J. Mech. Phys. Solids*, vol. 60, no. 1, pp. 120–138, Jan. 2012.

[35] L. Dorfmann and R. W. Ogden, *Nonlinear theory of electroelastic and magnetoelastic interactions*, vol. 9781461495. 2014.

[36] M. Behrooz and F. Gordaninejad, "Three-dimensional study of a one-way, flexible magnetorheological elastomer-based micro fluid transport system," *Smart Mater. Struct.*, vol. 25, no. 9, p. 95012, Sep. 2016.

[37] G. Schubert and P. Harrison, "Magnetic induction measurements and identification of the permeability of Magneto-Rheological Elastomers using finite element simulations," *J. Magn. Magn. Mater.*, vol. 404, pp. 205–214, Apr. 2016.

[38] A. K. Bastola, M. Paudel, and L. Li, "Magnetic circuit analysis to obtain the magnetic permeability of magnetorheological elastomers," *J. Intell. Mater. Syst. Struct.*, p. 1045389X1878104, Jun. 2018.

[39] V. R. Jayaneththi, K. C. Aw, and A. J. Mcdaid, "Wireless magnetic polymer actuator for implantable applications," in *IEEE/ASME International Conference on Advanced Intelligent Mechatronics, AIM*, 2017.

[40] G. A. Holzapfel, *Nonlinear Solid Mechanics: A Continuum Approach for Engineering*, vol. First Edit. 2000.

[41] D. Romeis, P. Metsch, M. Kästner, and M. Saphiannikova, "Theoretical models for magneto-sensitive elastomers: A comparison between continuum and dipole approaches," *Phys. Rev. E*, vol. 95, no. 4, p. 42501, Apr. 2017.

[42] J. Zeng, Y. Guo, Y. Li, J. Zhu, and J. Li, "Two-dimensional magnetic property measurement for magneto-rheological elastomer," *J. Appl. Phys.*, vol. 113, no. 17, p. 17A919, May 2013.

[43] R. W. Ogden, "Large Deformation Isotropic Elasticity - On the Correlation of Theory and Experiment for Incompressible Rubberlike Solids," *Proc. R. Soc. A Math. Phys. Eng. Sci.*, vol. 326, no. 1567, pp. 565–584, Feb. 1972.

[44] S.-H. Kim, J.-H. Choi, and S.-H. Lee, "Shape and dynamic behavior of nonmagnetic material immersed in magnetic nanofluid due to magnetic surface and body force density," in *2016 IEEE Conference on Electromagnetic Field Computation (CEFC)*, 2016, pp. 1–1.

[45] D. Güth, M. Schamoni, and J. Maas, "Magnetic fluid control for viscous loss reduction of high-speed MRF brakes and clutches with well-defined fail-safe behavior," *Smart Mater. Struct.*, vol. 22, no. 9, p. 94010, Sep. 2013.

[46] D. J. Griffiths, *Introduction to Electrodynamics*, Fourth. Pearson Education, 2014.

[47] M. Petit, A. Kedous-Lebouc, Y. Avenas, M. Tawk, and E. Artega, "Calculation and analysis of

local magnetic forces in ferrofluids."

[48] A. M. Winslow, "Numerical solution of the quasilinear poisson equation in a nonuniform triangle mesh," *J. Comput. Phys.*, vol. 1, no. 2, pp. 149–172, Nov. 1966.

[49] P. Deuflhard, "A modified Newton method for the solution of ill-conditioned systems of nonlinear equations with application to multiple shooting," *Numer. Math.*, vol. 22, no. 4, pp. 289–315, 1974.

[50] ASTM International., "ASTM D412-16 Standard Test Methods for Vulcanized Rubber and Thermoplastic Elastomers—Tension." ASTM International, West Conshohocken, PA, 2016.

[51] F. Delfino, A. Manella, P. Molfino, and M. Rossi, "Numerical calculation of total force upon permanent magnets using equivalent source methods," *COMPEL - Int. J. Comput. Math. Electr. Electron. Eng.*, vol. 20, no. 2, pp. 431–447, Jun. 2001.

[52] F. Delfino, "Some numerical aspects in electrodynamics of magnetic materials," *ICS Newsl.*, 2001.

[53] S.-H. Lee *et al.*, "Evaluation of the mechanical deformation in incompressible linear and nonlinear magnetic materials using various electromagnetic force density methods," *J. Appl. Phys.*, vol. 97, no. 10, p. 10E108, 2005.

[54] L. H. De Medeiros, G. Reyne, and G. Meunier, "Comparison of global force calculations on permanent magnets," *IEEE Trans. Magn.*, vol. 34, no. 5, pp. 3560–3563, 1998.